ELSEVIER

Journal of Alloys and Compounds 446–447 (2007) 212–217

Journal of ALLOYS AND COMPOUNDS

www.elsevier.com/locate/jallcom

A comparison of the evolution during the mechanical alloying of both a $MmNi_5$–Ni and a Mm–Ni mixtures: Stages of milling and microstructural characterization

M.R. Esquivel [a,b,*], G. Meyer [a,b]

[a] *Centro Atómico Bariloche, Comisión Nacional de Energía Atómica, Avenida Bustillo km 9.5, Bariloche, Río Negro 8400, Argentina*
[b] *Consejo Nacional de Investigaciones Científicas y Técnicas, Argentina*

Received 6 October 2006; received in revised form 18 January 2007; accepted 19 January 2007
Available online 25 January 2007

Abstract

The advantages attributed to hydride forming materials synthesized by either mechanical alloying (MA) or milling (MM) are related to an enhancement of the alloy conditioning previous to sorption of hydrogen, mainly due to the generation of defects and strain on the microstructure. This treatment can be done either after the synthesis by further MM of the alloy or simultaneously by MA of the constituents. To select the most suitable method, mixtures of Mm–Ni and $MmNi_5$–Ni were mechanically alloyed/milled in a low energy milling device. The changing of the microstructure during processing was analyzed by X-ray diffraction (XRD), scanning electron microscopy (SEM) and energy dispersive spectroscopy (EDS). The evolution of particle morphology and size were analyzed and the stages of alloying/milling were identified. The MA process of the Mm–Ni mixture occurs in four stages: initial, intermediate, final and completion. The MM process of the $MmNi_5$–Ni mixture occurs in two main stages, governed successively by fracture and cold welding, respectively. The final alloy condition, structure and microstructure are correlated to the evolution of each process.

Keywords: Rare earth alloys and compounds; Mechanical alloying; Intermetallics

1. Introduction

The thermodynamic and kinetic sorption properties of AB_5 alloys have been extensively studied in the last years. Some of the most relevant features of these alloys are summarized elsewhere [1,2]. Their application in hydrogen compression devices has attracted a renewed interest [3]. This feature along with an intrinsic versatility of lanthanides to occupy either as individual or alloyed the A site in AB_5's leaded to an increasing interest in new synthesis methods and conditioning treatments of these intermetallics for using in compression devices.

Intermetallic thermodynamic properties can be fitted to the device requirements by changing the composition of the A site. It can be done by replacing the site element by an expensive combination of pure lanthanides or by the cheaper Mischmetal (Mm). This synthesis can be successfully done by mechanical alloying (MA)/milling (MM) [4,5].

The introduction of defects and strain in the microstructure as a consequence of the milling process enhances the hydrogen sorption properties and a quicker activation of the intermetallic respect to those obtained by equilibrium methods such as direct melt casting. However, many of the studies performed using MA/MM were done using high energy mills [6–8]. Milling in these devices is so energetic that hinders the presence of the stages occurring during the evolution of this process. But these steps can be identified in a low energy mill where the development of the stages is slower and can be clearly observed and correlated to the intermetallic microstructure.

The possibility of applying this research work in both the scientific and industrial fields aimed the elaboration of this paper.

2. Experimental

Pure Ni (99.99%) (Sigma Aldrich) and drilled lumps of Mischmetal (99.7%) (Alpha Aesar) of nominal composition 52.0 wt.% Ce, 25.6 wt.% La, 16.9 wt.% Pr, 5.5 wt.% Nd. Mischmetal (Mm) composition was verified by neutron

* Corresponding author at: Centro Atómico Bariloche, Comisión Nacional de Energía Atómica, S.C. de Bariloche, Río Negro 8400, Argentina.
Tel.: +54 2944 445156/5197; fax: +54 2944 445299.
E-mail address: esquivel@cab.cnea.gov.ar (M.R. Esquivel).

0925-8388/$ – see front matter © 2007 Elsevier B.V. All rights reserved.
doi:10.1016/j.jallcom.2007.01.111

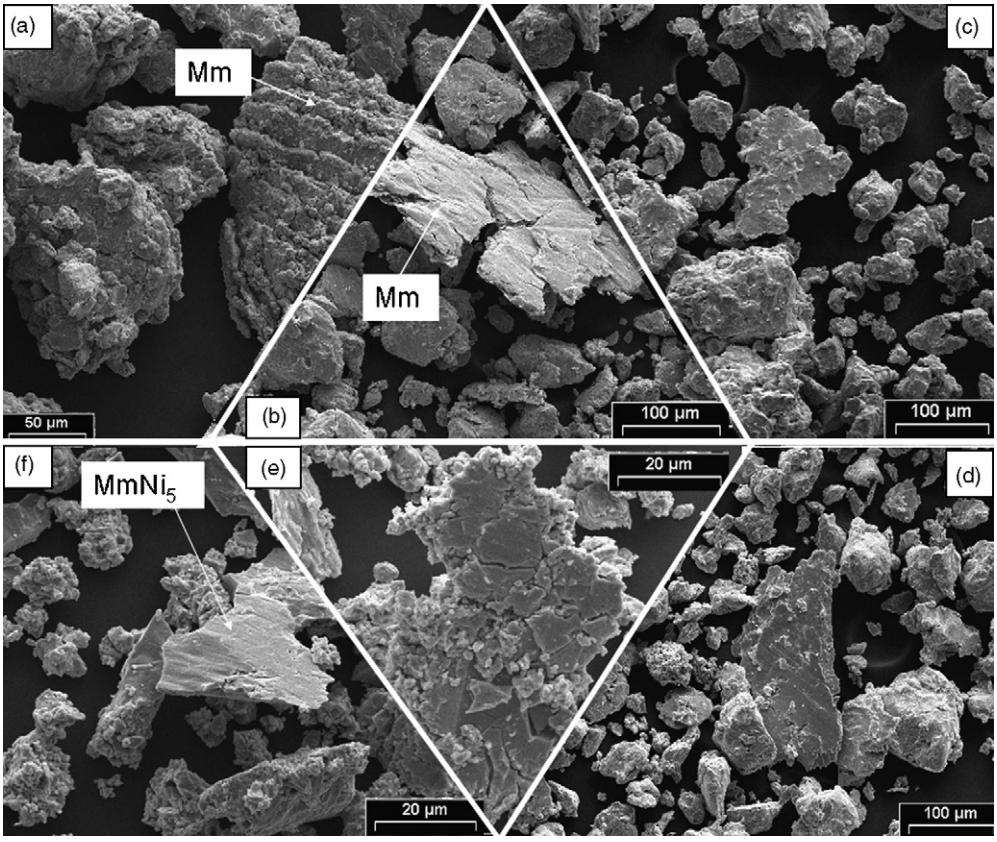

Fig. 1. Mosaic of SEM micrographs of Mm–Ni samples milled at different integrated milling times. (a) 2 h; (b) 5 h; (c) 10 h; (d) 20 h; (e) 40 h; (f) 100 h. Mm particles identified by EDS are labeled.

activation analysis (NAA) and energy dispersive spectroscopy (EDS). After synthesis of the intermetallic, the $MmNi_5$–Ni mixture was heated at 600 °C during 5 days to full crystallization. Mechanical alloying/milling were done under Ar atmosphere using a Uni-Ball-Mill II apparatus (Australian Scientific Instruments). Powder mixtures and steel balls were set in a stainless steel chamber under Ar atmosphere in a glove box. Oxygen level was monitored by a trace analyzer (Series 3000, Alpha Omega) and kept under 5 ppm to avoid material oxidation. The balls to powder mass relation was 33.5/1. In each case, representative amount of powder was withdrawn from chamber at different milling times inside a glove box and samples were analyzed by room temperature X-ray powder diffraction (XRD). Diffraction patterns were analyzed by the Rietveld method using DBWS software [9]. Particles size and morphology were observed by scanning electron microscopy (SEM).

3. Discussion and results

3.1. Mechanical alloying of Mm–Ni: microstructure and chemical homogeneity

A mosaic of samples withdrawn from chamber at different milling times is shown in Fig. 1. Fig. 1a shows a 2 h milled sample. Characteristic sawn tooth shape due to drill pretreatment of Mm is clearly observed. Mm particles were identified by EDS. Flower like Ni particles located over the Mm teeth were also identified by EDS. Fig. 1b shows a 5 h milled sample. Mm particles flatted by the impingement of the stainless steel balls are depicted. Evidences of fracture, typical of this stage [10], in the shape of a crack are also displayed. No tooth is present, only remaining marks, in the shape of a parallel track on the Mm surface, are left. There are still remaining individual Ni particles at this integrated milling time. Fig. 1c displays alloyed flat Mm–Ni particles. No homogeneous chemical composition is observed by EDS microanalysis at this stage. A 20 h milled sample is shown in Fig. 1d. Progressive cold welding is

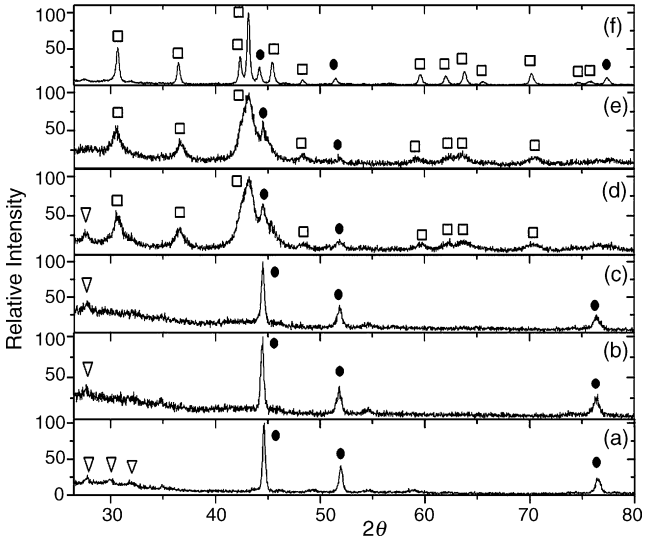

Fig. 2. Diffractograms of Mm–Ni samples milled at different integrated milling times. (a) 2 h; (b) 10 h; (c) 20 h; (d) 40 h; (e) 100 h. (f) Milled 100 h plus heating at 600 °C during 1 h. Ni diffraction lines are indicated in full circles. $MmNi_5$ diffraction lines are shown in full squares. Mm diffraction lines are indicated in inverted hollow triangles.

Table 1
Cell parameters and Rietveld refinements of both Mm–Ni and $MmNi_5$–Ni mixtures

	Cell parameters (Å)			Mass percentage		R_{wp}
	$MmNi_5$		Ni (*a*)	$MmNi_5$	Ni	
	a	*c*				
Fig. 2f	4.929	3.997	3.5727	76.19 ± 1.20	23.81 ± 3.70	15
Fig. 4b	4.915	3.984	3.5388	95.05 ± 0.32	4.95 ± 0.79	14
Fig. 4c	4.917	3.986	3.5396	95.07 ± 0.32	4.95 ± 0.79	16
Fig. 4d	4.917	3.989	3.5400	94.24 ± 0.05	5.76 ± 1.00	12
Fig. 4e	4.907	3.993	3.5342	92.42 ± 0.31	7.58 ± 2.00	10
Fig. 4f	4.893	4.001	3.5330	93.54 ± 0.23	6.56 ± 2.50	10
Fig. 4g	4.862	4.025	3.4400	92.22 ± 1.31	7.58 ± 5.00	14

R_{wp} stands for the goodness of the fit.

observed as usually at this step of the process [10]. Its presence is clearly observed in Fig. 1e where a homogeneous EDS identified $MmNi_5$ particle is depicted. Cold welded particles are also observed at 100 h of milling (Fig. 1f). Chemical identity and structure were verified by XRD. Some of the corresponding diffractograms are shown in Fig. 2. At shorter milling times, the diffraction lines of a combination of cubic and hexagonal Mm phases [11] and Ni diffraction lines (JCPDF Card number 040850) are observed (Fig. 2a–d). $MmNi_5$ diffraction lines are observed at 40 h (Fig. 2d) and 100 h (Fig. 2e), respectively in agreement with the EDS analysis of Fig. 1e–f. For comparison, the difractogram of the sample milled 100 h and heated at 600 °C during 1 h is shown in Fig. 2f. Rietveld refinement was used to quantify the mass percentage and crystalline parameters of the mixture. Summary of results is presented in Table 1. Calculation of crystallite size and strain introduced during milling is estimated from Ni diffraction lines by assuming empirically a Gauss distribution and Cauchy (Lorentz) component, respectively [12]. Instrumental broadening was calculated from reference pure Si. Results for both $MmNi_5$ and Ni are summarized in Table 2. As observed strain and crystallite size increases and decreases with milling, respectively.

3.2. Stages of mechanical alloying in this system

As observed in Figs. 1 and 2, the evolution of milling shows an increasing change in chemical composition and structure and particles morphology. A mosaic of SEM images displaying the presence of the different milling stages is shown in Fig. 3. *Initial stage* is observed up to 5 h. Particle size is decreased as milling progresses as observed in Fig. 3a and b and summarized in Table within Fig. 3. Particles morphology is greatly affected as correlated with Fig. 1a and b due to micro-forging product of stainless steel balls over particles. Chemical composition is not homogeneous as observed in Fig. 2a and b where Mm and Ni are still not alloyed.

Intemediate stage occurs between 10 and 20 h, both fracture and cold welding compete and initial particle morphology is changed, average particle size increases and cold welding is clearly observed on some particles surface as seen in Figs. 1d and 3c, d and quantified in Table within Fig. 3. Chemical homogeneity is not still reached (Fig. 2c) as typical of this stage [10], but the formation of a bump in the 30–40° range suggests the incipient formation of amorphous Mm–Ni structure.

Table 2
Strain and crystallite size of both Mm–Ni and $MmNi_5$–Ni mixtures at various milling times

Mixture milled	Element/intermetallic	Milling time (h)	Diffraction line (*h k l*),(2θ)	Crystallite size (Å)	Strain (%)
Mm–Ni	Ni	2	(1 1 1), (44.582)	727	0.027
		5	(1 1 1), (44.524)	754	0.028
		10	(1 1 1), (44.343)	559	0.037
		20	(1 1 1), (44.470)	548	0.037
		40	(1 1 1), (44.516)	342	0.060
		100	(1 1 1), (44.546)	112	–
	$MmNi_5$	40	(1 1 1), (42.944)	129	–
		100	(1 1 1), (42.970)	130	–
$MmNi_5$–Ni	Ni	2	(1 1 1), (44.327)	592	0.036
		5	(1 1 1), (44.270)	252	0.082
		10	(1 1 1), (44.225)	244	0.084
	$MmNi_5$	2	(1 1 1), (43.240)	599	0.035
		10	(1 1 1), (43.198)	329	0.065
		20	(1 1 1), (43.220)	216	0.098
		40	(1 1 1), (43.199)	128	0.100
		100	(1 1 1), (43.352)	130	0.150

Most intense lines were selected.

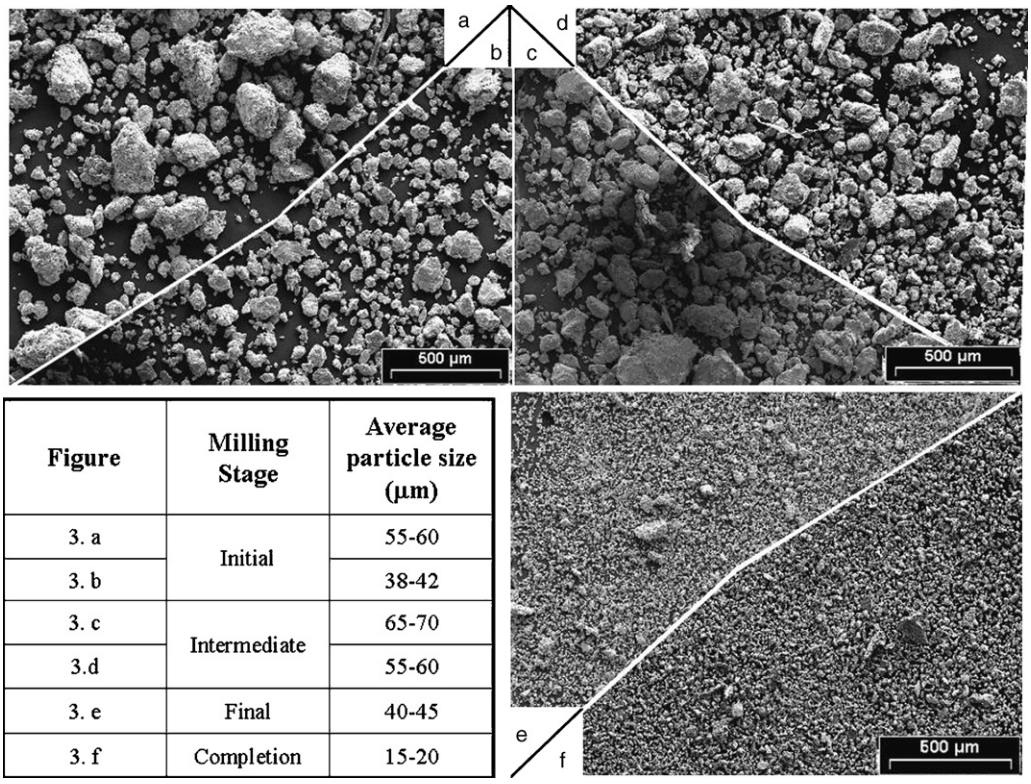

Figure	Milling Stage	Average particle size (μm)
3. a	Initial	55-60
3. b		38-42
3. c	Intermediate	65-70
3.d		55-60
3. e	Final	40-45
3. f	Completion	15-20

Fig. 3. Mosaic of SEM micrographs of Mm–Ni samples milled at different integrated milling times. (a) 2 h; (b) 5 h; (c) 10 h; (d) 20 h; (e) 40 h; (f) 100 h. Table in lower left corner summarizes the stages of milling and particle average size.

Final stage occurs at longer milling times between 20 and 40 h. The fracture-cold welding cycle is now dominated by the first process leading to a decrease on the average particle size as seen in Fig. 3e and Table within this figure. $MmNi_5$ is formed during this stage and the intermetallic and the remaining excess of Ni reach their final ratio in the mixture. At milling times longer than 40 h, typical *Completion stage* occurs [10] and particle size refinement is achieved leading to a decrement in particle size as observed by comparing Fig. 3e and f and no further chemical composition changes occur as observed by comparing Fig. 2d and e.

3.3. Mechanical milling of $MmNi_5$–Ni: microstructure and structure changes

A diffractogram series of $MmNi_5$–Ni samples extracted at different milling times is shown in Fig. 4. $MmNi_5$ and Ni crystalline parameters and mass percentages in the mixture are summarized in Table 1.

A broadening in peaks width as milling increases is observed. Quantification of the crystallite size decrease and strain increase for most intense diffraction peaks is summarized in Table 2.

3.4. Stages of mechanical milling in this system

Fig. 5 shows a mosaic of SEM micrographs of samples withdrawn from chamber at different milling times. As observed, the cycle of fracture and cold welding is governed by the first process at shorter times. (Fig. 5a–d), controlled by both of them an intermediate milling times (Fig. 5e) and dominated by the second at longer times (Fig. 5f–h). Since equilibrium species corresponding to the equivalent lanthanide (Ln)–Ni diagram are present, no changes on the chemical composition occur in agreement with the results of Fig. 4. This successive control of milling

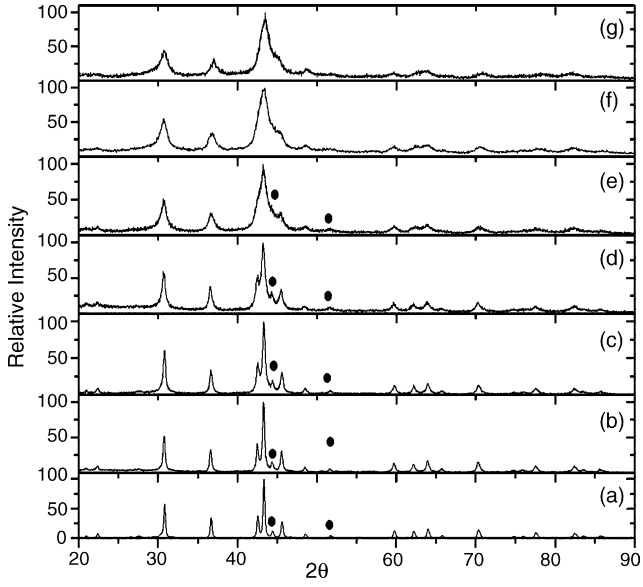

Fig. 4. Diffractograms of $MmNi_5$–Ni samples milled at different integrated milling times. (a) Initial; (b) 2 h; (c) 5 h; (d) 10 h; (e) 20 h; (f) 40 h; (g) 100 h. Ni diffraction lines are indicated by full circles. The other diffraction lines correspond to $MmNi_5$ [11].

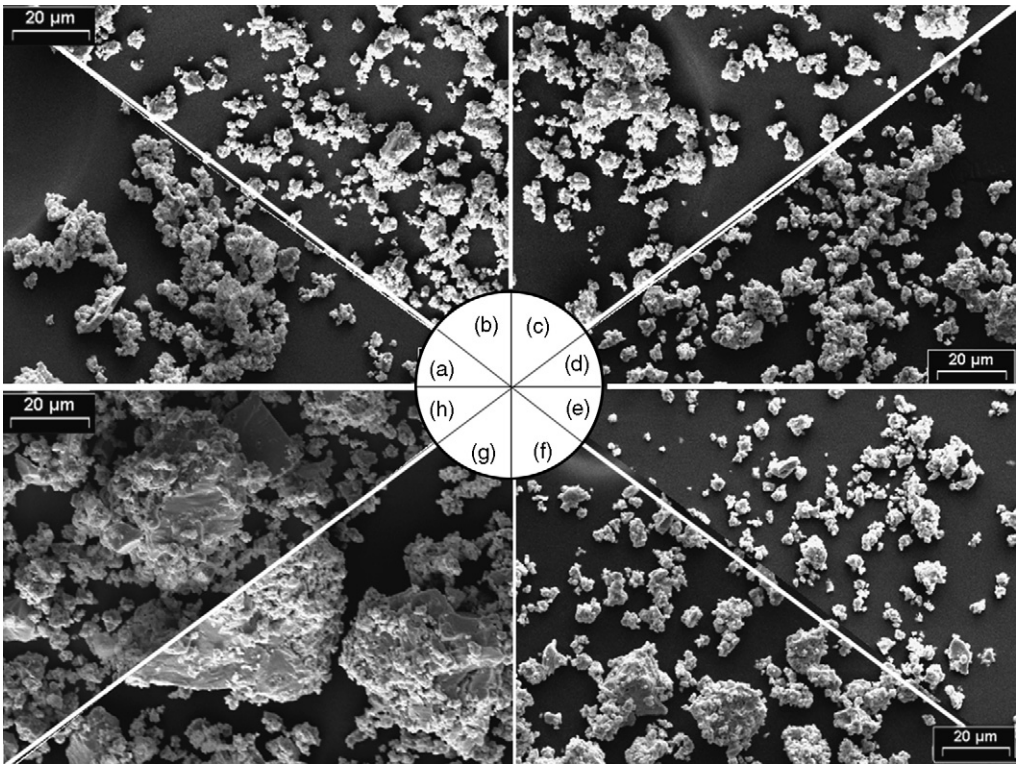

Fig. 5. Mosaic of SEM micrographs of $MmNi_5$–Ni samples milled at different integrated milling times. (a) Un milled; (b) 2 h; (c) 5 h; (d) 10 h; (e) 20 h; (f) 40 h; (g) 60 h; (h) 100 h.

stages was previously observed in a high energy milling device for the La–Ni system [6].

3.5. Comparison of the evolution and selection of the conditioning method

The Mm–Ni mixture MA evolves under the successive presence of four stages: *initial*, *intermediate*, *final* and *completion*. Changes in composition to fit the equilibrium species, $MmNi_5$ and Ni, are achieved during the process. The cycle of fracture and cold welding during the milling of $MmNi_5$–Ni mixture evolves trough three steps, the first dominated by fracture, the *second* involves a shared control between fracture and cold welding and the third is dominated by this last process. In both cases, the final $MmNi_5$ crystallite size achieved at 40 and 100 h is the same as seen in Table 1. Although a direct comparison of the strain of $MmNi_5$ lines can not be done because of the poor crystallinity of the samples, It is observed that the intermetallic and Ni present similar strain values and that Ni lines manifest a stronger effect in the second case, it can be concluded that the second mixture is strongly affected by mechanical milling at the same integrated milling time than the first one. This is probably because most of the energy applied to Mm–Ni system is lost by grinding of Mm as deduced from the bumpy formation of Mm–Ni in Fig. 2a–c and decrement of particle size of Fig. 1a–c. Although it seems that strain affects the $MmNi_5$–Ni mixture stronger than the Mm–Ni one, the volume cell parameter of the intermetallic is higher in the case of the Mm–Ni which suggests a better hydrogen interaction.

4. Conclusions

A comparison of Mm–Ni and $MmNi_5$–Ni initial mixtures was studied. The mechanisms of mechanical alloying/milling lead to similar crystallite size and particle size values at similar milling times in each case. Initial $MmNi_5$–Ni is strongly affected by mechanical milling reaching higher strain values as deduced from Ni diffraction lines. Nevertheless, $MmNi_5$ obtained from Mm–Ni by MA presents an easier one step synthesis-conditioning way of fabrication along with a higher volume cell parameter suggesting a better potential hydrogen interaction. Its weaker strain condition can be compensated by further milling of the final product. This subject is elucidated in an incoming paper work.

Acknowledgements

The authors wish to thank to the Agencia Nacional de Promoción Científica y Tecnológica of Argentina (Project No. PICT 12-15605), to the Consejo Nacional de Investigaciones Científicas y Técnicas of Argentina (Project No. PIP 6448) and to the Comisión Nacional de Energía Atómica of Argentina (Project No. PID 95-2) for partial financial support.

References

[1] P.S. Rudman, G.D. Sandrock, Annu. Rev. Mater. Sci. 12 (1982) 271–294.
[2] G. Sandrock, J. Alloys Compd. 293–295 (1999) 877–888.
[3] Z. Dehouche, N. Grimard, F. Laurencelle, J. Goyette, T.K. Bose, J. Alloys Compd. 399 (2005) 224–236.

[4] M. Jurczyk, W. Rajewski, W. Majchrzycki, G. Wójcik, J. Alloys Compd. 290 (1999) 262–264.
[5] M. Jurczyk, J. Alloys Compd. 307 (2000) 279–282.
[6] J.R. Ares, F. Cuevas, A. Percheron Guégan, Acta Mater. 53 (2005) 2157–2167.
[7] G. Liang, J. Huot, R. Scultz, J. Alloys Compd. 320 (2001) 133–139.
[8] S. Corré, M. Bououdina, N. Kuriyama, D. Fruchart, G. Adachi, J. Alloys Compd. 292 (1999) 166–173.
[9] R.A. Young, A.C. Larson, C.O. Paiva-Santos, J. Appl. Cryst. 28 (1995) 366–367.
[10] L. Lu, M.O. Lai, Mechanical Alloying, vol. 4, Kluwer Academic Publishers, Boston, 1998, pp. 69–153.
[11] M.R. Esquivel, F.C. Gennari, J.J. Andrade Gamboa, G. Meyer, Actas J SAM/CONAMET (2005), ISBN 987-22443-22-0-8.
[12] S. Enzo, E. Bonetti, I. Soletta, G. Cocco, J. Phys. D: Appl. Phys. 24 (1991) 209–216.